Non-invasive monitoring of cardiac contractility and sympathetic drive: Trans-Radial Electrical Bioimpedance Velocimetry (TREV)

Alexandra Stump[1*]

Caitlin Gregory[1*]

Viktoriya Babenko[1]

Elizabeth Rizor[1]

Tom Bullock[1,2]

Alan Macy[3]

Barry Giesbrecht[1,2]

Scott T Grafton[1,2]

Neil M Dundon[1,2,3]

*Contributed equally as first author

[1]Department of Psychological and Brain Sciences, University of California, Santa Barbara, CA 93106, USA
[2]Institute for Collaborative Biotechnologies, University of California, Santa Barbara, CA 93106, USA
[3]Department of Child and Adolescent Psychiatry, Psychotherapy and Psychosomatics, University of Freiburg, 79104 Freiburg, Germany
[4]BIOPAC Systems, Inc, Goleta, CA, USA.

Corresponding Author: neil.dundon@psych.ucsb.edu

Abstract

We describe methods and software resources for a bioimpedance measurement technique, "trans-radial electrical bioimpedance velocimetry" that allows for the non-invasive monitoring of relative cardiac contractility and stroke volume, proxies of sympathetic cardiac tone. In addition to describing the general recording methodology, which requires impedance measurements of the forearm, we provide open source Jupyter based software (operable on most computers) for deriving cardiac contractility from the impedance measurements. We demonstrate the ability of this bioimpedance measurement for tracking event related contractility in a maximal grip force production task. Critically, the results demonstrate both a reactive increase in cardiosympathetic drive with force production as well as a learned increase in drive prior to grip onset, consistent with allostatic autonomic regulation. The method and software should be of broad utility for investigations of event related cardio-sympathetic regulation in psychophysical studies.

Introduction

The cardiovascular system adapts quickly and dynamically in anticipation of and in response to a variety of stressors. Tracking these perturbations of sympathetic control by a measurement with high temporal resolution is a promising approach for identifying both physiological and psychological drivers of stress (Cieslak, et al., 2018). Bioimpedance methods, particularly impedance cardiography (ICG), have long been used to investigate the sympathetic branch of the autonomic nervous system to the heart by capturing electromechanical modulation of cardiovascular activity during cognitive tasks (Miller & Horvath, 1978). ICG uses a high frequency electrical current delivered via a total of 8 pairs of electrodes placed on the neck and thorax, while another pair of electrodes are required to record the electrocardigram. Using the combination of impedance cardiography and electrocardiography, a number of cardiodynamic parameters that are sensitive to sympathetic drive can be derived. These include intervallic parameters such as left ventricular ejection time (LVET) and pre-ejection period (PEP) as well as estimates of stroke volume (SV) and cardiac output (CO) based on idealized models of the thorax (Bernstein, 2009).

While ICG is a powerful approach, the method has drawbacks. Because the measurements are acquired across the thorax, the normal respiratory cycle introduces a complex set of confounds including changes of thoracic size and shape that undermine the application of ideal models. Furthermore, cyclic changes of intrathoracic pressure and venous return to the heart introduce added uncertainty in isolating sympathetic dynamics from other physiologic control variables. Pragmatically, motion artifacts and operational challenges related to applying electrodes to the naked torso pose additional limitations. More problematic has been the modeling of the resultant thoracic impedance waveform. The analysis depends on the identification of the b-point, a subtle inflection of the impedance wave corresponding to the opening of the aortic valve. Despite the development and distribution of semi-automated software tools by our lab for expediting the labeling of the b-point, we find that for many studies b-point

identification continues to require extensive hands-on expert quality control for labeling ambiguous time points. While the variability in labeling the b-point can be overcome by averaging heart beats over a sliding time window, this compromises the goal of measuring sympathetic responses on a fast time scale (Cieslak, et al., 2018).

Given the ongoing challenges of ICG analysis and the goal of characterizing cardiosympathetic drive on a beat-by-beat time scale, we have investigated other bioimpedance measurements besides ICG (Sel, Osman, & Jafari, 2021). Here we present a particularly promising method called Trans-Radial Electrical Bioimpedance Velocimetry (TREV) (Bernstein, Henry, Banet, & Dittrich, 2012). In contrast to ICG, TREV is a user-friendly approach that avoids many of the problems that result from acquiring signals across the thorax. Instead, impedance signals with TREV are measured across the length of the volar forearm. Changes of the impedance signal are directly related to a pressure wave propagating along the radial and ulnar arteries that arises with the opening of the aortic valve. In the following sections, we describe the underlying biomechanical and electrical properties of TREV that lead to the estimation of cardiac contractility. We demonstrate the utility of this approach with an isometric grip force task to capitalize on the known increase in sympathetic activation while humans apply their maximum grip force to a grip transducer (Richter, 2015; Richter, Gendolla, & Wright, 2016; Stanek & Richter, 2016; Stanek & Richter, 2021). We show that TREV is capable of capturing beat by beat allostatic anticipatory changes of the sympathetic nervous system, suggesting that participants can learn to develop a sympathetic response prior to movement onset. Finally, we provide signal processing software operable on most computers and a tutorial for streamlining the conversion of TREV impedance measurements into beat-by-beat estimates of contractility.

I. Background Physics and Physiology

Red blood cells and impedance

Several biophysical properties contribute to the changes of electrical impedance measured with TREV. Under static conditions (without blood flow or arterial pressure gradients), the red blood cells, constituting approximately 40% of blood volume in a vessel, will be randomly oriented. Due to the random orientation of the biconcave red blood cells, an increased resistance within the plasma is observed, as the artery exhibits a maximal level of electrical resistivity (Bernstein, 2009). During normal blood flow through the radial and ulnar arteries, the short axis of red blood cells aligns perpendicular to the flow axis. Additionally, impedance Z (measured in ohms/sec) and blood volume will vary as a function of velocity (v), which we assume remains constant along the measured segments of the two arteries. It is important to note that the denotation of Z in ohms per second is a departure from the typical usage of Z in other branches of physics where Z is expressed in units of ohms (Bernstein, Henry, Banet, & Dittrich, 2012).

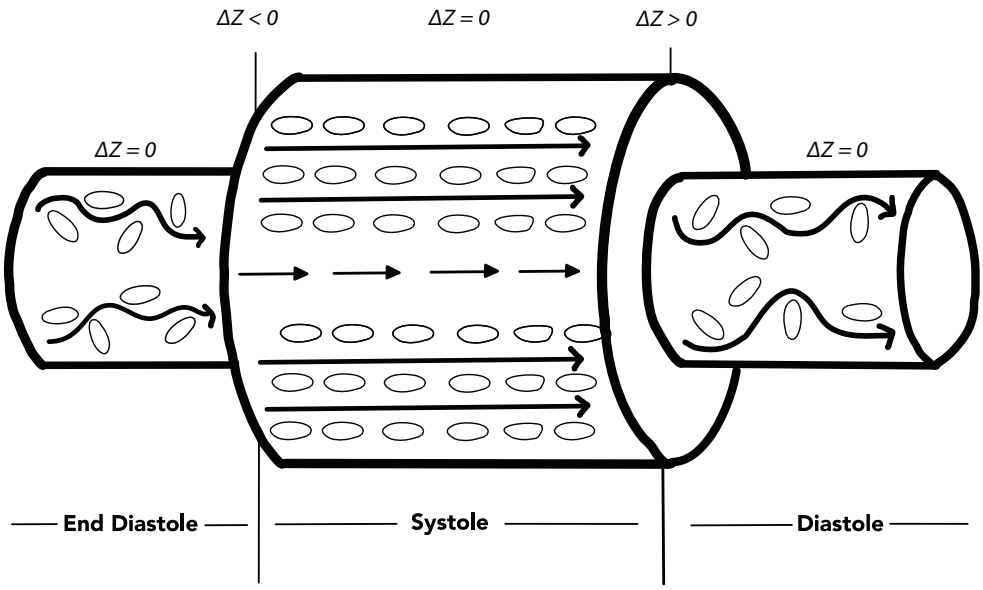

Figure 1: Pulsatile blood flow through the artery of the forearm. During systole, the pressure wave both dilates the blood vessel and rapidly aligns red blood cells, resulting in decreased impedance. Adapted from (Bernstein, 2009).

Generation of a pressure wave

During diastole of the cardiac cycle, the aortic valve is closed, isolating aortic blood pressure from intraventricular pressure as blood fills the ventricle, boosted by atrial contraction. With systole, the ventricular myocardium contracts, the mitral valve closes and isovolumic intraventricular pressure rapidly rises until pressure in the ventricle surpasses aortic pressure, at which point the aortic valve opens. A pressure surge occurs at this moment. This near instantaneous pressure wave is rapidly transmitted throughout the arterial vasculature. In a stiff pipe, this wave travels at a velocity of 1280 m/s. Because the vasculature, particularly the proximal aorta, is compliant, there is both a delay and dispersion of this pressure wave compared to a rigid pipe. With TREV, when this slightly delayed and dampened pressure wave arrives in the arteries of the forearm the red blood cells will further align as shown in Figure 1. The

net effect is a decrease in impedance *Z*. As shown in Figure 1 there can also be an increase in blood volume; however, changes in blood volume in the forearm vasculature are relatively minor.

Cardiac contractility, or the vigor with which the heart contracts, will determine in large part the intraventricular pressure that is generated during systole. As sympathetic activity increases, cardiac contractility also increases. Thus, contractility is a particularly useful variable of interest for tracking sympathetic dynamics in psychophysiological research. For a healthy individual at rest, end-diastolic ventricular volume will also impact intraventricular pressure and potentially influence the pressure wave and stroke velocity that change impedance. Critically, the greater the ventricular contractility, the higher the stroke velocity and change of impedance. To better characterize this change, we can take the derivative of stroke velocity which we can refer to as acceleration, measured as dZ/dt in units of ohms per second squared. In a single cardiac cycle, the maximum of the acceleration wave corresponds to the time at which the radial artery has the lowest resistivity. We can take the derivative of acceleration (in engineering, this is known as 'jerk'), to obtain contractility, (d^2Z/dt^2), in ohms per second cubed. This wave can be interpreted as the strength at which the acceleration is generated, which occurs at the moment the aortic valve opens, and reflects the maximal isovolumic ventricular pressure. In addition to contractility, stroke volume can also be calculated by integrating the normalized acceleration curve. A previous validation study demonstrates good correlation between cardiac MRI and TREV based estimates of stroke volume and cardiac output (Bernstein, et al., 2015)

The key benefit of TREV over ICG is that with the former, the measure is based on blood flow through the linear axially-oriented segments of the radial (and ulnar) artery as opposed to multi-oriented flow directions in the heart, aortic arch and heavily branching thoracic vasculature. The linear, longitudinal orientation of the radial and ulnar arteries in the forearm simplifies the relationship between impedance, blood flow and stroke velocity generated by the vigor of cardiac contractility. A similar relationship is not obtainable with ICG because the thoracic impedance measurement cannot distinguish

pressure-induced impedance changes in the aorta from those occurring in the ventricle, as both are within the field of measurement. Because of the limitations of impedance cardiography alone, the combination of ICG and EKG must be performed to derive measurements of sympathetic: PEP, LVET, SV, and CO. Thus, TREV's advantageous design comes from the ability to derive a direct measurement of sympathetic activation, contractility, without the usage of a 10-electrode ICG-EKG system. Additional information on the mathematical derivation of contractility, effect of compliance, and extension to estimations of stroke volume are available as a supplement that accompanies the Jupyter software described below.

II. Anticipatory changes of cardiac contractility with isometric force production

In this section we demonstrate changes in contractility associated with the isometric force produced by bilateral maximum strength hand grips. Using repeated measures of grips, it is possible to observe the development of an anticipatory change in contractility prior to grip onset, consistent with allostatic regulation by the autonomic nervous system (McEwen & Wingfield, 2003).

Materials and Methods

Participants and experimental overview

Thirty-one healthy humans (19 females) participated in the study after providing informed consent in accordance with the University of California, Santa Barbara (UCSB) Institutional Review Board. Participants self-reported no cardiovascular abnormalities. The average age of participants was 23.4 years. One participant was excluded due to excessively noisy data, leaving a final sample of n = 30. Participants were compensated $10/hour plus a potential $10 bonus depending on task performance (see Grip Task below).

Participants performed two blocks of a maximum grip task (Grip Task), each block corresponding to three sequential grips of one hand and then the other (with hand order randomized across subjects).

Three simultaneous physiological timeseries were recorded in each block. The first timeseries was time-varying cardiac impedance derived from TREV, with electrodes attached to the forearm contralateral to the hand administering grips (Figure 2). The second timeseries was a standard electrocardiogram (EKG). The last timeseries recorded the continuous respiration cycle with an abdominal belt.

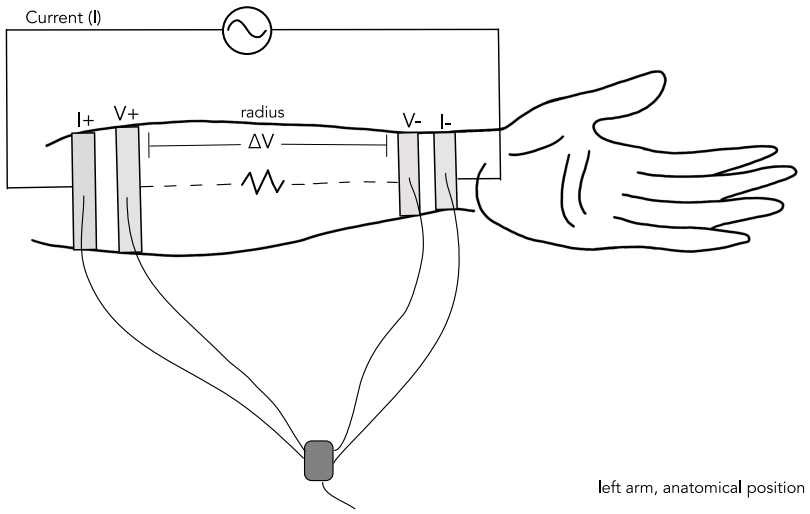

Figure 2: Electrode placement of trans-radial electrical bioimpedance velocimetry system. Four electrodes placed on the forearm; two outer current electrodes (I+ and I-) and two inner voltage sensing electrodes (V+ and V-). I+ and I- create an alternating current field (*I)* through the forearm, and any changes in forearm impedance are directly correlated to changes in voltage Δ*V* between V+ and V-.

Recording Apparatus

TREV electrodes were amplified by an NICO100D (BIOPAC Systems, Inc., Goleta, CA, USA) smart amplifier. A current field is applied across the forearm by means of a constant magnitude, high frequency (50-100 kHz) low amplitude alternating current (4 mA RMS). The constant current (*I*) is introduced through the two outer electrodes (I^+ and I^-) and the resulting voltage (*V*) is measured via the inner electrodes (V^+ and V^-). Using Ohm's Law, we can use the voltage differential *V* and applied current *I* to calculate impedance *Z* (measured in ohms):

$$Z(t) = V(t) / I(t)$$

Here, *I* and *V* are the root mean square values of the known current and measured voltage. Because the magnitude of the current *I* is constant, any change in voltage *V* over time will vary in direct proportion to changes in impedance *Z*. This method allows us to capture moment-to-moment fluctuations in bioimpedance, which directly correlate with perturbations in the autonomic nervous system.

Electrocardiogram electrodes were amplified by an ECG100D (BIOPAC Systems, Inc.) smart amplifier. Respiration cycle was recorded using a TSD221-MRI (BIOPAC Systems, Inc.) respiration belt. Force exerted in the Grip Task was recorded using an SS56L (BIOPAC Systems, Inc.) grip bulb. All continuous signals were integrated using an MP160 (BIOPAC Systems, Inc.) amplifier and processed online using BIOPAC AcqKnowledge software (BIOPAC Systems, Inc.). Visual stimuli were presented on a 21" monitor using Microsoft PowerPoint. Offline preprocessing of recorded timeseries was conducted using the Moving Ensemble Analysis Pipeline (MEAP) and MATLAB (Cieslak, et al., 2018). Bayes models were fitted using No U-Turn sampling (NUTS) Hamiltonian Monte Carlo, fitted with PyMC3 Python3 functions (Salvatier, Wiecki, & Fonnesbeck, 2016).

General Procedure

All data were recorded in a single session lasting approximately 45 minutes (including initial equipment setup). Participants first washed their hands and forearms with water and regular soap to remove dirt or oily residues. In a private setup room, an experimenter then placed four TREV electrodes on the forearm contralateral to the grip hand of the first block (see Grip Task, below). Two electrodes were placed ventrally on the distal region of the forearm, just below where the wrist meets the hand, and two electrodes on the proximal region of the forearm, just below where the elbow meets the forearm (Figure 2). Each electrode pair was spaced one centimeter apart. TREV electrodes are bioimpedance strip electrodes (BIOPAC EL526 - size 1.3cm x 16.5cm). These electrodes establish circumferential equipotential lines at the four electrode locations.

Next, the experimenter placed two EKG electrodes on the participant's chest: one below the right collarbone and one where the deltoid meets the chest. Participants were then brought to the testing room, electrodes were connected to the associated amplifiers, a respiration belt was placed around the participant's abdomen, and they were seated at the testing table 3 feet from a computer screen. Once seated, participants were taught how to properly hold and squeeze the grip bulb, with the tubing facing down and in a manner that involved the whole hand. Participants were also instructed to maintain the same posture and to keep their arms relaxed, still, and in the same positioning on the table throughout the entirety of the experiment.

Grip Task

The experimenter first asked participants to grip the bulb as hard as possible with each hand, recording each maximal value (max thresholds). Participants then performed two blocks of three trials, gripping with the opposite hand in each block (block-hand order was determined with uniform (p=0.50) probability for each participant). After recording participants' maximum forces (max thresholds; above), the experimenter then explained the experimental protocol, which is depicted in Figure 3. Prior to the start of the first block of trials, participants were instructed to sit idly for three minutes to acclimate to the exam room. The experimenter then quietly entered the room to start the physiological recording and associated computer task. Once the experiment started, the experimenter departed the room. Trials began with an on-screen countdown timer, where participants were instructed to look at the screen through a two-minute rest period. At the end of the rest period, a "go" cue would appear, signaling to the participants to squeeze the bulb maximally for two seconds. The countdown period of the next trial's rest period then immediately began. This cycle continued for two more grips. At the end of the third trial on each block, a timer counted down to a visual stimulus that instructed participants to ring a bell to alert the experimenter they had finished. Each of the three trials was therefore preceded and followed by a two-minute rest. To incentivize participants to grip with maximum strength, we imposed a bonus

system, whereby participants who reached a threshold of ± 0.04 Kg/m^2 of their hand-specific max-thresholds on all three grips would win a $10 bonus. The experimenter disclosed this rule to participants after recording the max thresholds and did not inform participants if they had achieved the bonus until after all testing was completed. After completing the first block, the experimenter transferred the TREV electrodes to the other arm and the grip task was repeated.

Figure 3. Within block timing of grip task and rest. This structure was performed for each hand.

Cardiovascular preprocessing

During recording, the AcqKnowledge software was used to apply an online lowpass filter (max cutoff = 20 Hz) to the raw impedance timeseries *Z(t)* recorded by the TREV electrodes and then calculated as a continuous estimation of acceleration. This raw contractility timeseries was then imported together with the raw EKG and respiration timeseries to the MEAP software for minimal offline processing. MEAP first automatically labelled the R-peaks of the EKG timeseries, which we used as an index for the moment in time to define each individual heartbeat. We next used these R-peak time indices to extract epochs spanning +/-350 ms around each heartbeat from the raw contractility timeseries (contractility epochs). MEAP also computed estimates of heart-rate at each beat from the R-peaks. MEAP outputs were then transferred to MATLAB, where the maximum amplitude in each contractility epoch was computed as an estimation of each heartbeat's contractility (beat-wise contractility timeseries). Then, separately for each subject, and each block, we conducted an additional regression procedure (Dundon, et al., 2020; Dundon, Shapiro, Babenko, Okafor, & Grafton, 2021) to remove the additional confounding effects of heart-rate and respiration from the beat-wise contractility

timeseries. Using a multiple regression model, we regressed the vector beat-wise contractility as a function of an intercept and three regressors: (i) the phase of respiration at each heartbeat, (ii) the amplitude of respiration at each heartbeat and (iii) the heartrate at each heartbeat. To down sample each regressor to beat-wise estimates, we used the value from raw timeseries closest to the time of each R-peaks. We added the estimated intercept to the residuals from this model as the "residualized" contractility timeseries, i.e., with the effects of the above three regressors removed. Given both between-subject and within-subject variation in heart rate, we next applied temporal resampling of each block's residualized timeseries to allow meaningful comparisons across participants. For this, we used one-dimensional linear interpolation across time to recreate residualized timeseries sampled at equal time intervals. Specifically, we took 479 estimates, spaced exactly one second apart, from 2 seconds post block onset until 480 seconds post block onset (interpolated contractility timeseries). Finally, these interpolated contractility timeseries were normalized as a *t*-statistic, i.e., each interpolated contractility estimate expressed as a t-statistic relative to the timeseries's remaining 478 values. We refer to this *t*-statistic-normalized timeseries from now on as the "contractility" timeseries. A grand average contractility timeseries across participants, separately for each block, is presented in Figure 4.

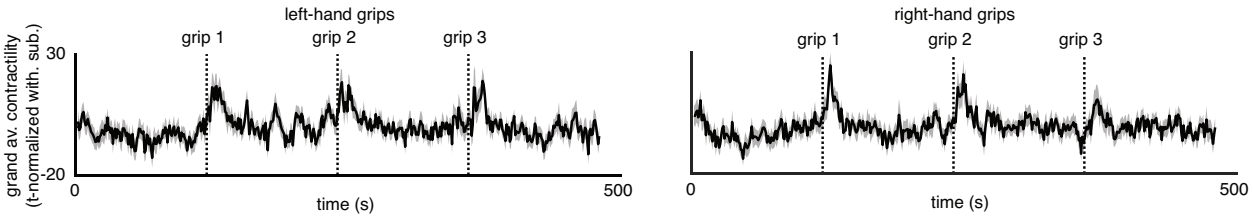

Figure 4: Grand average time series of contractility across participants for left and right hand blocks of trials.

Bayesian modeling framework

The primary objective of this analyses was to determine whether TREV could reliably capture increases in group-level contractility that corresponded to the events in the grip task, either in response to, or in anticipation of a grip. For this, we used a hierarchical Bayesian framework which hypothesized

that the (n=30) group distribution of contractility estimates at each timepoint (*t*) formed a Student's T distribution, $T(t) \sim$ Student's $T(\mu(t), \sigma(t), \nu)$. We formally considered contractility to have increased beyond baseline at a given moment where the estimated mean of a timepoint's distribution ($\mu(t)$) credibly exceeded the mean across all timepoints (M_{μ}). M_{μ} is itself fitted in the same model as the mean of a hierarchical Gaussian distribution (G_{μ}) which constrains estimates of each $\mu(t)$ by serving as their prior ($G_{\mu} \sim N(M_{\mu}, S_{\mu})$). Given how Bayes theorem ascribes joint probabilities to both the prior and the observed data in posterior estimates, this distributional hierarchical framework is inherently conservative with respect to type one error for each estimate of $\mu(t)$. For example, if most values for $\mu(t)$ are within a tight range (as we would expect in a dataset of contractility values with long rest periods between grips), the hierarchical distribution will be characterized by a more certain mean and low variance (low value of S_{μ}), which would then serve as a strict prior on $\mu(t)$ estimates, biasing them toward the group mean (i.e., a nail that stands out gets hammered in). This hierarchical framework therefore requires strong evidence before any $\mu(t)$ is formally accepted as a credible departure. In other words, in a context requiring multiple hypothesis tests, the hierarchical Bayesian framework imposes an adjustment to the level of evidence needed for credible effects, where the data itself determines that level of adjustment instead of an arbitrary criterion (e.g., Bonferroni).

We fitted a hierarchical model separately for blocks where grip was administered with the right and left hand. In each case, the specific free parameters of our model were: $\mu(t)$ and $\sigma(t)$, i.e., the 479 timepoint-specific mean and standard deviation parameters for group-level SNS distributions at each timepoint across each block. We did not fit the nu parameter hierarchically and assigned it the same uninformed prior ($\nu=1$) in each model. As mentioned above, each $\mu(t)$ parameter was constrained by a hierarchical Gaussian distribution (G_{μ}) with free parameters M_{μ} and S_{μ} corresponding respectively to its mean and standard deviation. M_{μ} was assigned an uninformed Gaussian prior, $N(0,1)$, while S_{μ} was assigned an uninformed half-Gaussian prior (forcing values to be positive), half$N(1)$. Each

sigma(t) was also constrained by hierarchical Gaussian distribution (G_{sigma}), which respectively used an uninformed Gaussian and half-Gaussian prior for its two free parameters, i.e., its mean ($M_{sigma} \sim N(0,1)$) and standard deviation ($S_{sigma} \sim \text{half}N(1)$). We formally compared each mu(t) posterior with that of the M_{mu} by computing the minimum-width Bayesian credible interval (Highest Density Interval (HDI)) of mu(t) - M_{mu} and only considered strong evidence of a departure at each timepoint, i.e., where resulting HDIs did not contain zero.

Contractility timeseries were z-score normalized prior to fitting across all participants. Each model's posterior distributions were sampled across four chains of 5000 samples (20000 total), after burning an initial 5000 samples per chain to tune the sampler's step-size to reach 0.95 acceptance. We estimated HDIs using the default setting in the arviz package (Kumar, Carroll, Hartikainen, & Martin, 2019).

Sliding window rate of change

We performed a sliding window deterministic regression to enumerate the rate of change in contractility at each point in our timeseries. At each timepoint we estimated the rate of change in contractility over the ensuing 20 seconds of the timeseries. Specifically, for each timepoint (t) we fitted a distribution of coefficients ($B(t)$), containing five thousand coefficients ($b(k)$), where each $b(k)$ estimated the relation between an arbitrary time vector [1,…,20] and independent draws from the proceeding 20 posteriors of mu, i.e., the 20-element vector [[*mu(t)](k),…, [mu(t+19)](k)*]. To identify credibly positive rates of change, we tested whether 97% of each deterministic distribution ($B(t)$) was above zero.

Results

We tested whether a thorax-independent monitor of cardiac impedance (TREV) could reliably describe fluctuations in cardiac contractility that credibly exceed baseline as human participants perform a task known to drive increased cardiovascular sympathetic stress. Thirty participants completed both blocks of three incentivized max-intensity grips, with rest periods of two minutes both between each grip

and following the final grip. Participants showed strong motivation to grip at maximum intensity, supported by 29 out of 30 achieving a bonus payment (contingent on beating their predetermined max threshold) with at least one hand, and 21 out of 30 achieving the bonus payment with both. Figure 5 depicts exemplar contractility for two heartbeats from a single subject, one in the rest phase prior to the second grip with their right hand and another in the grip's immediate aftermath.

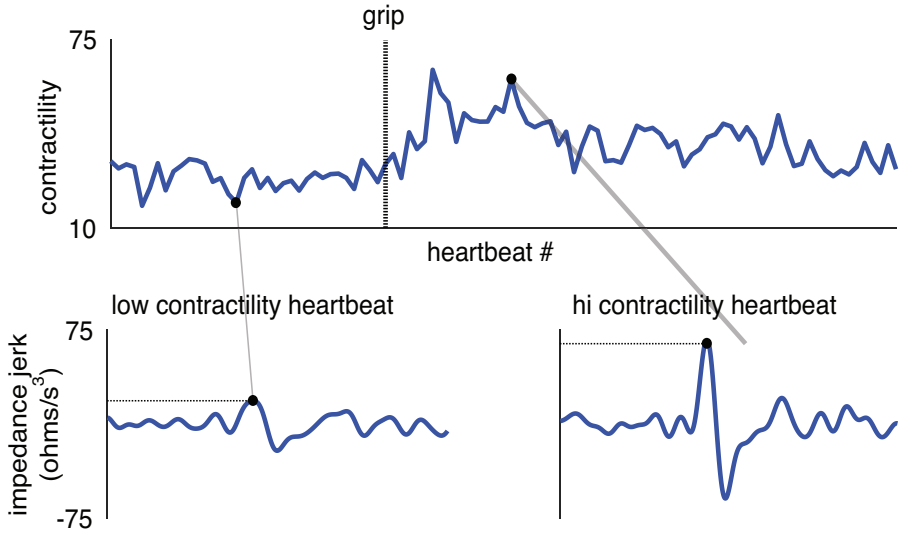

Figure 5: Top row is a sample timeseries of contractility estimated at 100 heartbeats. Bottom row shows how contractility is estimated from impedance jerk timeseries at two single heartbeats.

After linear resampling to temporally align contractility across participants and normalizing each block separately as a t-statistic, group-level contractility in temporal approximation to each grip was assessed. The results of the hierarchical Bayesian model fitted to contractility timeseries accompanying left-hand grips are depicted in the left panel of Figure 6. TREV reliably captured contractility exceeding baseline following grips with the left hand. Left hand grips were accompanied by credible baseline departure in seconds after grip onset at grip 1: [11, 12, 13, 15], grip 2: [-8, 5, 10, 11, 13] and grip 3: [8, 12, 13, 14, 15]. Each grip was therefore accompanied by at least 4 individual seconds of credible baseline departure. Departures mostly followed the grips and never followed a grip by more than 15

seconds. Each grip was associated with at least two consecutive seconds of baseline departure, with grip 3 associated with the longest sustained peak contractility (four consecutive points).

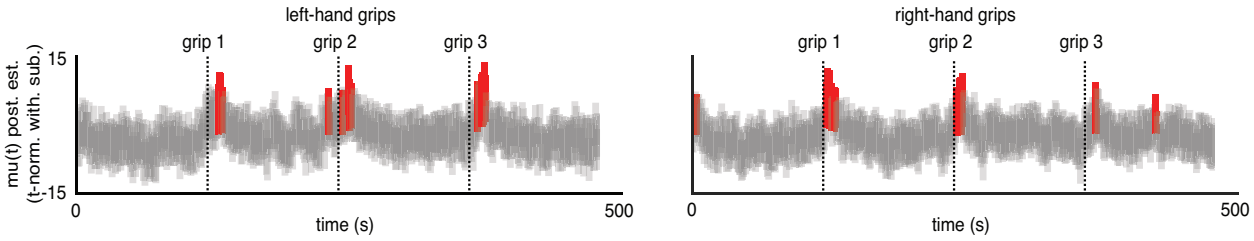

Figure 6. Results of hierarchical Bayesian model depicting credible departures from baseline contractility (in red) for left and right hand grips.

The results of the hierarchical Bayesian model fitted to contractility timeseries accompanying right-hand grips are depicted in the right panel of Figure 6. Right-hand grips were accompanied by credible baseline departure after grip onset (in seconds) for grip 1: [-114, 5, 6, 7, 8, 9, 12, 13], grip 2: [4, 5, 6, 7, 8, 9] and grip 3: [11, 66]. Discounting the two outliers (preceding grip 1 and following grip 3), each grip was therefore accompanied by at least 1 second of credible baseline departure. Departures all followed the grips and never followed a grip by more than 13 seconds. Grip 2 was associated with the longest sustained peak contractility (six consecutive points). TREV again appeared to reliably capture contractility exceeding baseline following grips with the right hand, although a pair of outliers were present and the duration of peak contractility seemed to abate over the course of the three grips.

Sliding window rate of change

As depicted in Figure 7, for both the left and right-hand grips, the rate of change was credibly positive at numerous timepoints in the series preceding each grip. For the left hand, the earliest of these credible pre-grip changes occurred at *t*=62, i.e., 58 seconds prior to the first grip; at *t*=185, i.e., 55 seconds prior to the second grip; and at *t*=349, i.e., 11 seconds prior to the third grip. For the right hand, the earliest of these credible pre-grip changes occurred at *t*=45, i.e., 75 seconds prior to the first grip; at *t*=178, i.e., 62 seconds prior to the second grip; and at *t*=348, i.e., 12 seconds prior to the third

grip. Interestingly, therefore, we observed a trend in both hands, whereby the rate of change became credibly positive much closer to the initiation of the grip by the third grip, consistent with the allostatic principle of participants learning task requirements and reserving a potentially expensive increase in cardiac contractility until the time it was most critically needed.

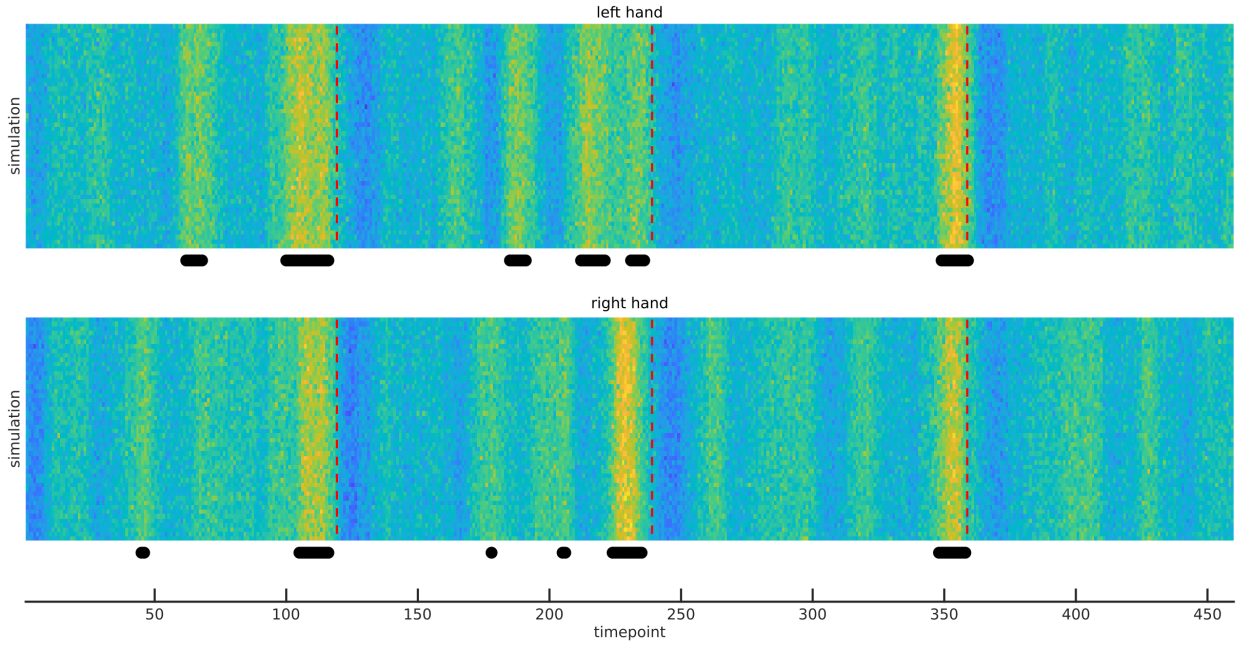

Figure 7. Sliding window rate-of-change. Each column of raster plots are 50 samples from distributions of regression coefficients measuring change in contractility over next 20-second window. Yellow colors are positive (increasing contractility). Markers below each panel reflect timepoints when 97% of distribution is positive, i.e., credibly positive increase in contractility.

Discussion

There is expanding interest across multiple human research disciplines in robustly capturing event-related perturbations of the sympathetic stress response. Consequently, there a need for new assays of cardiac contractility that both reduce preparatory requirements and offer increased signal strength in the face of background noise. In this study we used a novel trans-radial electrical bioimpedance velocimetry device (TREV), attached to the forearm of human participants, and investigated whether it could reliably capture changes in group-level contractility that corresponded to events known to increase sympathetic drive, a max grip task (Grip Task). We observed that TREV

electrodes can be applied relatively quickly with minimal training and preparation, and can even be repositioned (from one arm to the other) efficiently between blocks of a task. We further observed TREV to register easy, visually identifiable beat-to-beat signals from the radial and ulnar artery corresponding to the third derivative of the measured impedance wave. In preprocessing, we could readily control for potential confounding effects of respiratory activity and heart rate on beat-wise contractility timeseries. Then, using a hierarchical Bayesian framework, we observed these contractility timeseries to reliably depart baseline at key events in the Grip Task. Remarkably, these departures were seen at the single-trial level across participants (i.e., without averaging across trials). We therefore conclude that TREV offers an exciting development in cardiac autonomic stress research for human researchers interested in event-related capture of cardiac contractility.

We employed a data-driven analysis framework, which used the entire timeseries of data recorded across sessions, to determine when contractility estimated by TREV credibly exceeded baseline fluctuations. The primary advantage of this framework is that it removed all need to impose arbitrary criteria on grip events or contractility activity, i.e., a priori deciding epochs around task events to refine analysis, or a priori deciding a criterion that constituted "credibly exceeding baseline". The analysis was not assisted by any averaging across events to reduce signal-to-noise. The hierarchical Bayesian framework also imposed conservativeness with respect to credible departures from baseline across a large number of hypothesis tests. We nonetheless revealed reliable group-level increases in contractility at each of the six grips executed by participants. A significant sympathetic response to the physical challenge imposed by the grip task is consistent with motivational intensity theory. This theory posits that the sympathetic response should scale with the level of task difficulty, an effect which has been observed in both cognitive and grip tasks (see: Richter, Gendolla, & Wright, 2016, for a review).

Note that our criterion for baseline was the average value across all datapoints in the timeseries, which theoretically incorporates all preparatory increases in sympathetic activity leading up to grip

execution. When we employed a slope-based analysis strategy, we additionally observed credible anticipatory changes of contractility just prior to grip onset for all trials and with either hand. This observation is consistent with the role of the sympathetic nervous system in allostatic regulation, providing just enough input and just in time (McEwen & Wingfield, 2003).

In conclusion, we observed that thorax-independent TREV reliably captures contractility increases to individual events and offers considerable advantages for capturing event-related cardiac responses in more generalized real-world task settings. Such capture of contractility signals has the potential to greatly contribute toward improving our knowledge of how humans synchronize sympathetic state while monitoring broader state information, allowing us to develop more holistic technologies for human-machine integration that can assist with situational awareness, maneuverability and decision making.

III. Jupyter based signal processing software

In the following section, we describe public domain signal processing software operable on any Unix based system (Mac OS, Linux) and a tutorial for streamlining the conversion of TREV impedance measurements into beat-by-beat estimates of contractility. The software, SCOT: Semi-automated Contractility estimates from Ohmic impedance measured with TREV, uses the Jupyter Noteboook and is downloadable at https://github.com/caitgregory/SCOT. Unless otherwise specified, the pipeline uses the Tkinter package to manage all GUI interactions and Matplotlib (Hunter, 2007) to manage plots. It is currently configured to interact with output files from AcqKnowledge (BIOPAC); however, it theoretically could be amended to work with other file formats. Users can fully test or replicate this pipeline by downloading an example data set from the tutorial at https://github.com/caitgregory/SCOT/blob/main/tutorial.md. The example data were recorded for 45 minutes during a simultaneous fMRI recording while human participants performed speeded reaches

with a joystick. These data were minimally preprocessed during acquisition using AcqKnowledge Software by performing an online lowpass filter (max cutoff = 20 Hz) and the calculation of stroke acceleration, *dZ/dt*.

Pipeline Processing

In four largely automated steps, users are able to import the data (Jupyter Notebook, Cell 1), identify beat by beat time intervals (Cells 2 and 3), estimate cardiac contractility at each beat (Cell 4), and remove artifacts related to heart rate and respiratory activity (Cell 5).

Cell 1 of the Jupyter Notebook loads the data via a GUI (Figure 8) using the bioread functions (Vack, 2023). (To replicate the pipeline, users can use the AcqKnowledge file IV_301_1.acq). The resulting menu allows users to specify the appropriate acceleration channel and respiration channels defined during the acquisition. Note that the pipeline imports the stroke acceleration channel (which provides more easily identifiable peaks relative to noise. Here, users can also specify if the acceleration channel or the respiration channel require a FIR low-pass filter. We have preset the cutoff of these filters in the notebook at 22.5 Hz and 0.35 Hz, respectively. The filters use a Hamming window and a length computed by the convention used in freely available packages for processing electrophysiological data (MNE; (Gramfort, et al., 2013). Specifically, we construct a filter using the firwin function (SciPy; (Virtanen, et al., 2020) with a length of *N*. *N* is computed with 3.3 x 1/*tb*. Here, *tb* is a transition bandwidth which is the minimum value between *f1* and *f2*, where *f1* is the maximum between one quarter of the specified cutoff and 2, and *f2* is the Nyquist frequency minus the specified cutoff. We then apply the filter using the lfilter function (SciPy) and adjust the phase shift by discarding the first *N/2* samples of data and readjusting the time points. The user exits out of the menu which initiates the above steps. Depending on the length of the data this initial import could take a couple of minutes. A notice will appear in the cell output once this step is complete.

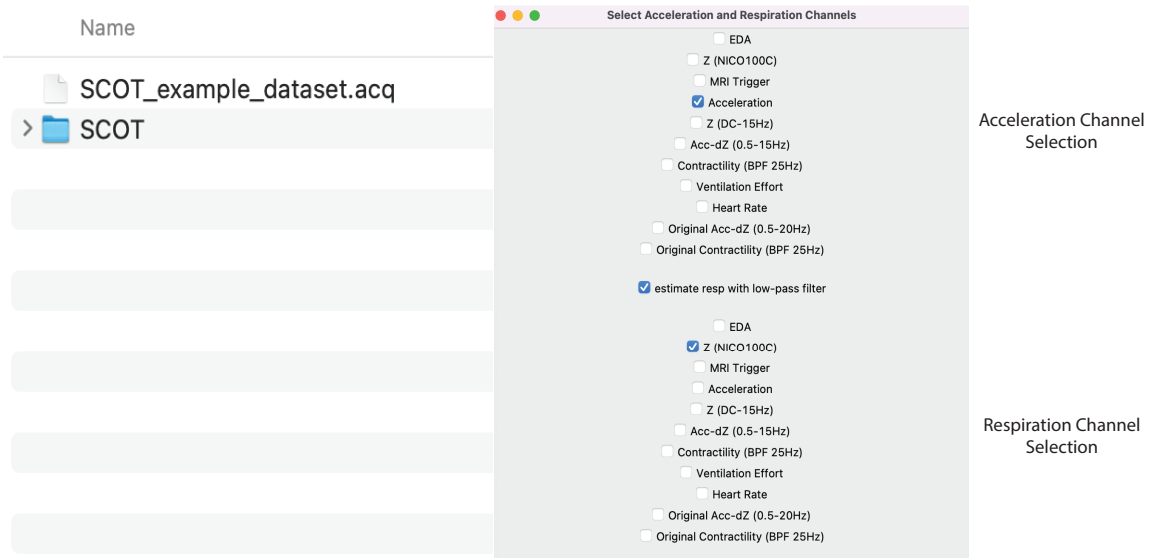

Figure 8: Cell 1 GUI.

Cells 2 and 3 identify the time interval between each heartbeat by finding peaks in the acceleration timeseries. As noted above, the acceleration timeseries (dZ/dt) is more robust to noise than the contractility timeseries (d^2Z/dt^2), allowing for an easier identification of peaks. The program uses the SciPy findpeaks function which we preset to find peaks spaced at least 0.5 seconds apart (equivalent to a heart rate of 120 BPM). In Cell 2, (Figure 9) users can visually inspect a 20 second portion of the acceleration timeseries at time to identify a minimum threshold for peak amplitude, which they manually input. In addition to the minimum spacing, this peak amplitude threshold acts as an extra automated control against spurious peak identification. On the sample data set, we selected a minimum threshold value of 0.5.

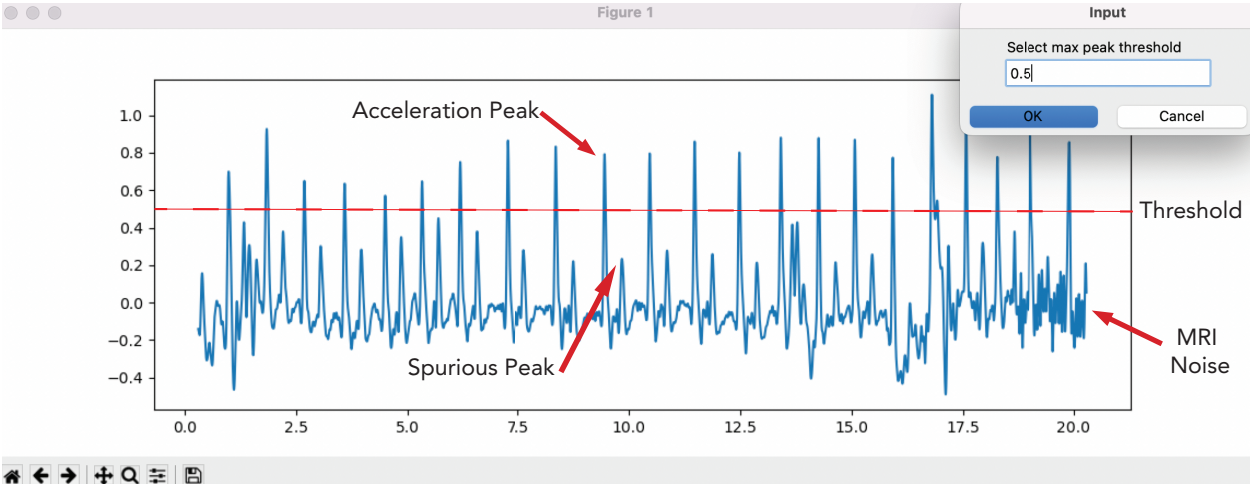

Figure 9: GUI for cell 2. Note the peak threshold is inputted as 0.5. This threshold value helps avoid flutter between acceleration peaks. The participant has a premature ventricular contraction at time 16.5s (causing a reduction of contractility due to reduced ventricular filling). Also note the onset of MRI scanning at 18 seconds. Despite the associated MRI associated noise, acceleration peaks are still visible and robust.

Cell 3 (Figure 10) allows users to manually add and remove heart beats via an interactive timeseries of the acceleration waveform. Users can scroll through the data and identify any peaks that the program may have missed or mis-labeled. There are three keyboard options that allow the user to edit the pre-determined time points of the peaks. Using a two-button mouse, or equivalent keystrokes and clicks for a one-button mouse, a left click will add a peak and a right click will remove a peak. If is there is noise in the signal at any point or the user is unsure where exactly the peak should go, the user can press m + left click. Here, the script performs a moving ensemble average of the two previous and two consecutive peaks to determine the location of the peak of interest.

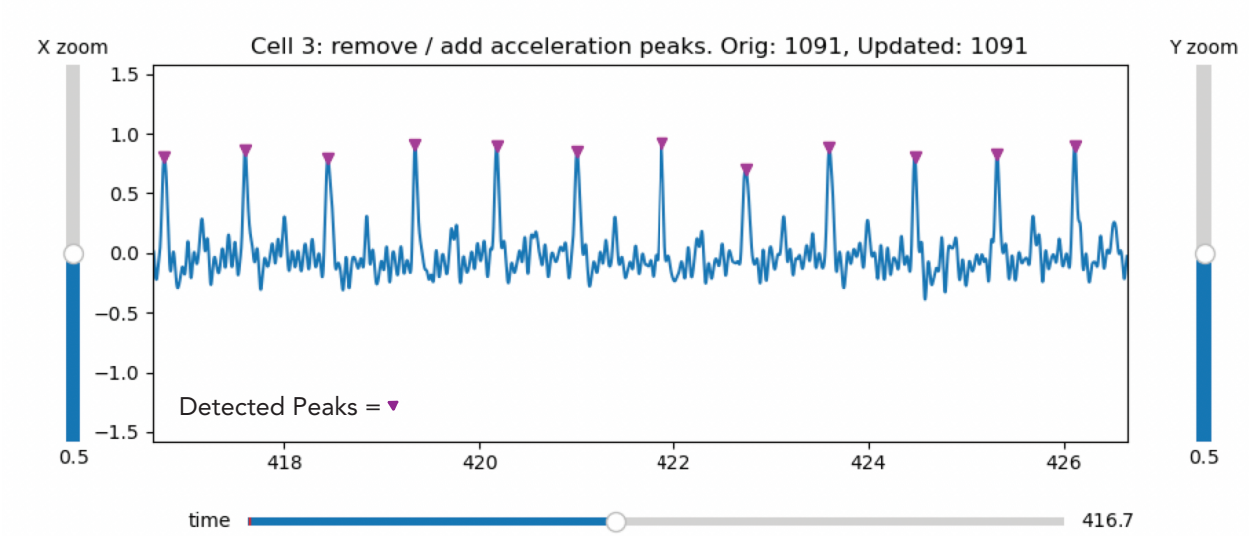

Figure 10: Cell 3 GUI. The acceleration time series plotted over time with detected peaks. The user is able to use the slider along the bottom of the graph to scroll through the data and adjust the peak location as needed.

Cell 4 (Figure 11) plots the contractility timeseries (the derivative of acceleration). Note that in cell 3 we found the maximum values of the acceleration timeseries, i.e., the critical values such that $d^2Z/dt^2 = 0$. Given that maximum acceleration is reached after peak contractility, the time points of peaks identified in cells 2 and 3 need to be adjusted backward in time. We accordingly search for maximum contractility amplitude in the time window spanning 250 ms prior to the identified acceleration peak. Users can scroll through the data and manually adjust the identified peak amplitude if necessary. Note that in this cell we are interested in peak contractility amplitude values rather than time points.

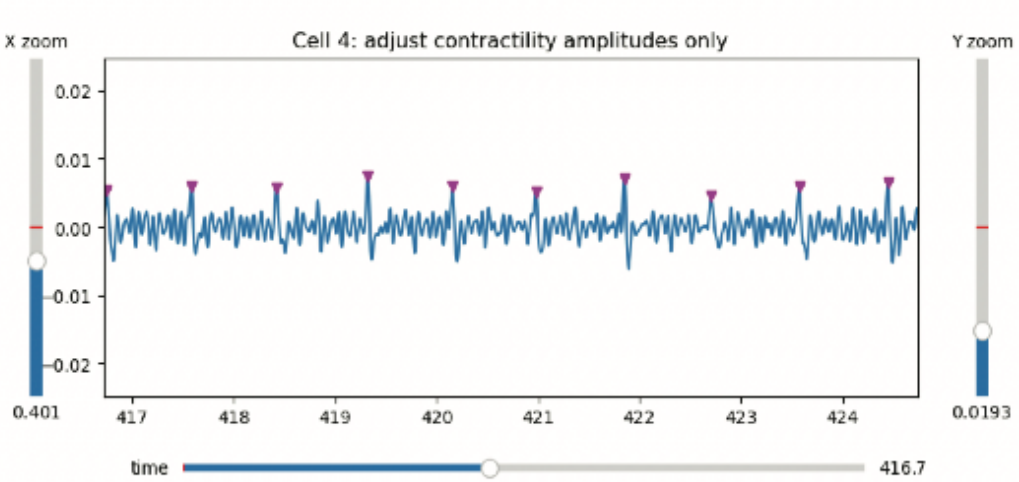

Figure 11: Cell 4 GUI. The contractility timeseries plotted over time.

Lastly, Cell 5 removes the influence of heart rate and respiration from the contractility estimates using the residualizing method described in the methods section above. Briefly, a multiple regression was conducted where contractility is modeled as a function of the heart rate, respiratory amount, and respiratory cycle at each heartbeat. Heart rate is computed from the inter-beat intervals identified in cell 3. Respiratory amount and cycle are identified by first finding each consecutive cosine-like segment in the specified respiration timeseries. *Y*-axis values (i.e. respiration amount) of each segment are demeaned while *x*-axis values (i.e., respiration phase) are normalized between 0 and 2π. We then extract the respiratory amount and phase values closest to each heartbeat. Prior to the regression, each regressor is *z*-scored. We output the residuals of the regression model as the contractility estimates with the effects of heart rate and respiration removed. Once completed, data are outputted into a csv file with each row corresponding to a heartbeat, and columns with the time of each heartbeat (relative to the beginning of the recording) and the contractility amplitude. By default, the csv will be named the same as the input AcqKnowledge file with the csv extension; however, users can change this through a GUI.

Acknowledgements

Supported by the Institute for Collaborative Biotechnologies under Cooperative Agreement W911NF-19-2-0026, contract W911NF-19-D-0001, and grant W911NF-16-1-0474, all from the Army Research Office. The content of the information does not necessarily reflect the position or the policy of the Government and no official endorsement should be inferred.

519 References

520 Bernstein, D.P. (2009). Impedance cardiography: Pulsatile blood flow and the biophysical and
521 electrodynamic basis for the stroke volume equations. *J Electrical Bioimpedance*, **1**, 2-17.
522 Bernstein, D.P., Henry, I.C., Banet, M.J., & Dittrich, T. (2012). Stroke volume obtained by electrical
523 interrogation of the brachial artery: transbrachial electrical bioimpedance velocimetry.
524 *Physiological Measurement*, **33**, 629-649.
525 Bernstein, D.P., Henry, I.C., Lemmens, H.J., Chaltas, J.L., DeMaria, A.N., Moon, J.B., & Kahn, A.M.
526 (2015). Validation of stroke volume and cardiac output by electrical interrogation of the brachial
527 artery in normals: assessment of strengths, limitations, and sources of error. Journal of Clinical
528 Monitoring and Computing, 29, 789-800.
529 Cieslak, M., Ryan, W.S., Babenko, V., Erro, H., Rathbun, Z.M., Meiring, W., Kelsey, R.M., Blascovich, J., &
530 Grafton, S.T. (2018). Quantifying rapid changes in cardiovascular state with a moving ensemble
531 average. *Psychophysiology*, **55**.
532 Dundon, N.M., Garrett, N., Babenko, V., Cieslak, M., Daw, N.D., & Grafton, S.T. (2020). Sympathetic
533 involvement in time-constrained sequential foraging. *Cognitive, affective & behavioral*
534 *neuroscience*, **20**, 730-745.
535 Dundon, N.M., Shapiro, A.D., Babenko, V., Okafor, G.N., & Grafton, S.T. (2021). Ventromedial Prefrontal
536 Cortex Activity and Sympathetic Allostasis During Value-Based Ambivalence. *Frontiers in*
537 *behavioral neuroscience*, **15**, 615796.
538 Gramfort, A., Luessi, M., Larson, E., Engemann, D., Strohmeier, D., Brodbeck, C., Goj, R., Jas, M.,
539 Brooks, T., Parkkonen, L., & Hämäläinen, M. (2013). MEG and EEG data analysis with MNE-
540 Python. *Frontiers in neuroscience*, **7**.
541 Hunter, J.D. (2007). Matplotlib: A 2D Graphics Environment. *Computing in Science & Engineering*, **9**, 90-
542 95.
543 Kumar, R., Carroll, C., Hartikainen, A., & Martin, O. (2019). ArviZ a unified library for exploratory analysis
544 of Bayesian models in Python. *J Open Source Softw*, **4**, 1143.
545 McEwen, B.S., & Wingfield, J.C. (2003). The concept of allostasis in biology and biomedicine. *Horm*
546 *Behav*, **43**, 2-15.
547 Miller, J.C., & Horvath, S.M. (1978). Impedance cardiography. *Psychophysiology*, **15**, 80-91.
548 Richter, M. (2015). Goal pursuit and energy conservation: energy investment increases with task demand
549 but does not equal it. *Motivation and Emotion*, **39**, 25-33.
550 Richter, M., Gendolla, G.H.E., & Wright, R.A. (2016). Three Decades of Research on Motivational
551 Intensity Theory: What We Have Learned About Effort and What We Still Don't Know. *Advances*
552 *in Motivation Science* (**Vol. 3**, pp. 149-186): Elsevier.
553 Salvatier, J., Wiecki, T.V., & Fonnesbeck, C. (2016). Probabilistic programming in Python using PyMC3.
554 *PeerJ Computer Science*, **2**, e55.
555 Sel, K., Osman, D., & Jafari, R. (2021). Non-Invasive Cardiac and Respiratory Activity Assessment From
556 Various Human Body Locations Using Bioimpedance. *IEEE Open J Eng Med Biol*, **2**, 210-217.
557 Stanek, J., & Richter, M. (2016). Evidence against the primacy of energy conservation: Exerted force in
558 possible and impossible handgrip tasks. *Motivation Science*, **2**, 49-65.
559 Stanek, J.C., & Richter, M. (2021). Energy investment and motivation: The additive impact of task
560 demand and reward value on exerted force in hand grip tasks. *Motivation and Emotion*, **45**, 131-
561 145.
562 Vack, N. (2023). bioread 3.0.1.Python Package Index. https://pypi.org/project/bioread.
563 Virtanen, P., Gommers, R., Oliphant, T.E., Haberland, M., Reddy, T., Cournapeau, D., Burovski, E.,
564 Peterson, P., Weckesser, W., Bright, J., van der Walt, S.J., Brett, M., Wilson, J., Millman, K.J.,

Mayorov, N., Nelson, A.R.J., Jones, E., Kern, R., Larson, E., Carey, C.J., Polat, İ., Feng, Y., Moore, E.W., VanderPlas, J., Laxalde, D., Perktold, J., Cimrman, R., Henriksen, I., Quintero, E.A., Harris, C.R., Archibald, A.M., Ribeiro, A.H., Pedregosa, F., van Mulbregt, P., Vijaykumar, A., Bardelli, A.P., Rothberg, A., Hilboll, A., Kloeckner, A., Scopatz, A., Lee, A., Rokem, A., Woods, C.N., Fulton, C., Masson, C., Häggström, C., Fitzgerald, C., Nicholson, D.A., Hagen, D.R., Pasechnik, D.V., Olivetti, E., Martin, E., Wieser, E., Silva, F., Lenders, F., Wilhelm, F., Young, G., Price, G.A., Ingold, G.-L., Allen, G.E., Lee, G.R., Audren, H., Probst, I., Dietrich, J.P., Silterra, J., Webber, J.T., Slavič, J., Nothman, J., Buchner, J., Kulick, J., Schönberger, J.L., de Miranda Cardoso, J.V., Reimer, J., Harrington, J., Rodríguez, J.L.C., Nunez-Iglesias, J., Kuczynski, J., Tritz, K., Thoma, M., Newville, M., Kümmerer, M., Bolingbroke, M., Tartre, M., Pak, M., Smith, N.J., Nowaczyk, N., Shebanov, N., Pavlyk, O., Brodtkorb, P.A., Lee, P., McGibbon, R.T., Feldbauer, R., Lewis, S., Tygier, S., Sievert, S., Vigna, S., Peterson, S., More, S., Pudlik, T., Oshima, T. (2020). SciPy 1.0: fundamental algorithms for scientific computing in Python. *Nature methods*, **17**, 261-272.